Proceedings of FUELCELL2005
Third International Conference on Fuel Cell Science, Engineering and Technology
May 23-25, 2005, Ypsilanti, Michigan, USA

FUELCELL2005-74050

ANALYSIS, MODELING, AND VALIDATION FOR THE THERMAL DYNAMICS OF A POLYMER ELECTROLYTE MEMBRANE FUEL CELL SYSTEM

Eric A. Müller
Measurement and Control Laboratory
Swiss Federal Institute of Technology Zurich (ETH)
Zurich, Switzerland
Email: mueller@imrt.mavt.ethz.ch

Anna G. Stefanopoulou
Fuel Cell Control Systems Laboratory
The University of Michigan
Ann Arbor, Michigan, 48109
Email: annastef@umich.edu

ABSTRACT

A control-oriented mathematical model of a polymer electrolyte membrane (PEM) fuel cell stack is developed and experimentally verified. The model predicts the bulk fuel cell transient temperature and voltage as a function of the current drawn and the inlet coolant conditions. The model enables thermal control synthesis and optimization and can be used for estimating the system performance. Unlike other existing thermal models, it includes the gas supply system, which is assumed to be capable of controlling perfectly the excess air and hydrogen ratio. The fuel cell voltage is calculated quasi-statically. Measurement data of a 1.25 kW, 24-cell fuel cell stack with an integrated membrane-type humidification section is used to identify the system parameters and to validate the performance of the simulation model. The predicted thermal response is verified during typical variations in load, coolant flow, and coolant temperature.

A first-law control volume analysis is performed to separate the relevant from the negligible contributions to the thermal dynamics and to determine the sensitivity of the energy balance to sensor errors and system parameter deviations.

NOMENCLATURE

A	Area [m^2]
A_{Active}	Active area [m^2]
C, C_p, C_{p0}	Specific heat [J/(kg K)]
E	Thermodynamic potential [V]
F	Faraday constant [A s]
$\dot{H}$	Enthalpy flow rate [W]
h	Convective heat transfer coefficient [W/(m^2K)]
h	Mass specific enthalpy [J/kg]
h_f^0	Mass specific enthalpy of formation [J/kg]
h_{fg}	Mass specific evaporation enthalpy [J/kg]
I	Electric current [A]
i	Electric current density [A/m^2]
K_h	Parameter of the heat transfer coefficient model
k_p	Nozzle constant of cathode channel [m s]
k_T	Cathode temperature parameter [W/K]
M	Molecular mass [kg/mol]
m	Mass [kg]
$\dot{m}$	Mass flow rate [kg/s]
n_{Cells}	Number of fuel cells [$-$]
P	Power [W]
p	Pressure [Pa]
Δp_{AnCa}	Pressure difference anode-cathode [Pa]
$\dot{Q}$	Heat flow rate [W]
S, s	Sensitivity
T	Temperature [K]
t	Time [s]
U	Internal energy [J]
V	Voltage [V]
δ_h	Parameter of the heat transfer coefficient model
ε	Emissivity [$-$]
λ_m	Membrane water content [$-$]
λ_{Air}	Air excess ratio [$-$]
ν	Overvoltage [V]
ξ	Parameter or signal value
σ	Stefan-Boltzmann constant [W/(m^2K^4)]

φ	Relative humidity [−]

Subscripts and Superscripts

Act	Activation
Amb	Ambient
B	Fuel cell system body
Cell	Fuel cell
Conc	Concentration
Conv	Convection
DI	Deionized water (coolant)
El	Electric
Evap	Evaporation
Excess	Non-reacting part of moist air flow
g	Gaseous
H_2	Hydrogen
H_2O	Water
HM	Humidification section
In	Inlet
Leak	Hydrogen flow lost through leakage
Liq, l	Liquid
mAir	Moist air
mH_2	Moist hydrogen
O_2	Oxygen
Ohm	Ohmic
Out	Outlet
Prod	Product
PS	Power section
Purge	Moist hydrogen flow purged
Rad	Radiation
Reac	Reaction
St	Stack
Syst	Fuel cell system

INTRODUCTION

Fuel cells (FC) are considered for automotive propulsion, electricity generation, and back-up power supplies. Virtually all applications have demanding transient requirements, especially during start-up and shutdown. A fast warm-up is a particularly critical task for every type of fuel cell because it typically defines the time period before any load can be supported. Even for low-temperature fuel cells such as the polymer electrolyte membrane (PEM) fuel cells, thermal management is necessary. The heat associated with the range of power needed for a typical passenger vehicle or a residential power supply cannot be passively dissipated by convection and radiation through the external surfaces of the FC. Consistent low-temperature (80 °C) operation thus requires a cooling system similar to the one used in internal combustion engines. The low temperature difference between the FC and the environment limits the effectiveness of the heat transfer from the coolant to the ambient and requires either a large radiator surface area or many cooling fans. Hence, a sophisticated controller of the fuel cell temperature becomes vitally important to ensure optimal system performance. For example, fast warm-up might require optimally controlled coolant flow. The control-oriented model should, thus, capture the effects of the cooling flow to the heat exchange process. During this warm-up period heat might be externally supplied for a short period. To minimize the external power requirements the control algorithm needs to optimize the amount and the rate of the heat delivery. To achieve this task systematically and consistently, a model of how the coolant temperature affects the bulk FC temperature is required. Although various modeling approaches of different levels of complexity have been proposed recently [1–4], these studies focus on performance analysis or system parameter optimization. The prior models involve cumbersome measurements, and have not been tested though variations in coolant flow, temperature and stack power.

The objective of this study was to derive a control-oriented mathematical model of the fuel cell system dynamics which can be used to forecast system performance as well as for thermal control development and optimization. The model should be easy to parameterize and it should predict the system temperature and the stack voltage as a function of just the coolant inlet conditions and the electrical current demand.

This paper first describes the 1.25 kW, 24-cell fuel cell system investigated and the setup of the test bench experiment. A first-law control volume analysis is performed and an energy and a water mass balance are evaluated for a set of experimental data recorded on the test bench. The control volume analysis is first verified and briefly discussed. In particular, a differentiation of relevant and negligible contributions to the thermal dynamics is made. The control volume analysis serves also as a basis for a sensitivity analysis which rates the impact of sensor errors or parameter uncertainties on the energy balance. Based on these investigations, the structure of a control-oriented lumped-parameter model is proposed. The model includes the gas supply system and accounts for the heat released by the chemical reaction, the vapor and product water flow enthalpies at cathode, including humidification, the surface heat losses, and the heat transferred to the deionized water of the coolant circuit. An existing static electrochemical model is used to calculate the fuel cell voltage and the gas supply system is assumed statically and perfectly controlled. The equations are derived and possible simplifications are explained. Where necessary, system parameters are identified with measurement data recorded on the test bench. Finally, the model is implemented and its prediction is validated with two different sets of experimental data.

FUEL CELL SYSTEM INVESTIGATED

Figure 1 shows the instrumented stack installed on the test station at the University of Michigan's Fuel Cell Control Labora-

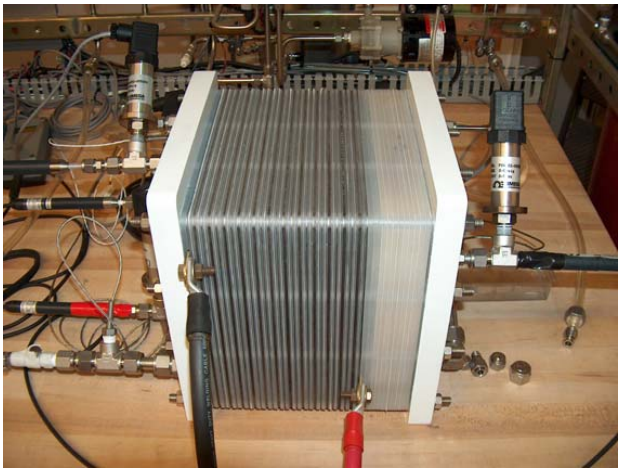

Figure 1. TEST BENCH: 1.25 KW, 24-CELL FUEL CELL STACK WITH AN INTEGRATED MEMBRANE-TYPE HUMIDIFICATION SECTION.

tory. The stack has 24 PEM fuel cells with GORE™ PRIMEA® series 56 membrane electrode assemblies (MEAs). The stack was designed and assembled at the Schatz Energy Research Center at Humboldt State University. Its MEAs have 0.4 mg/cm^2 and 0.6 mg/cm^2 platinum loading on the anode and cathode, respectively. The catalyst support is carbon black. To diffuse gas from the flow fields to the membrane, double-sided, hydrophobic, version 3 Etek™ ELATs® were used. The flow fields are comprised of machined graphite plates. The stack contains an internal humidification section that diffuses water vapor after the power section coolant loop to the incoming air through a GORE™ SELECT® membrane. There are two fuel cells between cooling plates in the power section.

The stack can produce 1.25 kW continuous power at less than 600 mA/cm^2. It is designed for operation at low temperatures ($<70\,^\circ$C), and at low gauge pressures (<12 kPa in the cathode and 14–34 kPa in the anode).

Experimental Setup

Protruding from the stack endplates in Fig. 1 are the transducers for relative humidity, temperature, and pressure. Their location is also shown in the schematic diagram of Fig. 2. The inlet coolant flow rate (location 1 in Fig. 2) is measured with a McMillan 101-8 Flo-Sensor with a range of 0–5 slm[1] and an accuracy of ± 0.02 slm. Two resistance temperature devices (RTD) with a range of -40–$85\,^\circ$C and an accuracy of $\pm 0.3\,^\circ$C measure the coolant temperatures at the inlet of the power section and the outlet of the humidification section (locations 1 and 2 in Fig. 2). An MKS type 1559A air flow controller (co-located sensor) with a range of $20-200$ slm, an accuracy of $\pm$ 2 slm, and a response time of 0.5 s is installed upstream of the air inlet (location 3 in Fig. 2). A Hastings HFM201 hydrogen mass flow meter with a range of 0–100 slm, ± 1 slm, and a response time of 2 s is installed upstream of the anode inlet (location 6 in Fig. 2). Four relative humidity (RH) sensors are installed in the inlets and outlets of the anode and cathode manifold within the stack (locations 4–7 in Fig. 2). The RH sensors are capacitive-based Rotronic SP05 probes with an integrated transmitter and a resistance temperature device (RTD). The RH sensor range is 0–100% with an accuracy of ± 1.5%. Three Omega PX4202–005G5V pressure transducers with a range of 0–5 psig, an accuracy of ± 0.012 psig and a response time of 10 ms are used at the locations 4–6 in Fig. 2. The sensor specifications were provided by the manufacturers and have not been independently verified. The current drawn from the stack is controlled and measured by a Dynaload RBL488 electronic load with a range of 0–500 A (± 0.015 A). Individual cell voltages are measured with 0–1200 mV/cell (± 1 mV/cell) and added together to calculate the stack voltage.

The data acquisition system is based on PCI DAQ boards with signal conditioning 5B backplane hardware and LabVIEW™ software. Data logging occurs at 2 Hz or a higher frequency, depending on the task being executed.

The fuel cell operates on a test station with integrated controls, diagnostics, and safety mechanisms. The air control system regulates the air flow at a desired stoichiometric level (200–400%) or at a fixed air flow value. The MKS air flow controller handles dry air supplied by an Atlas-Copco SF1–4 stationary oil-free air scroll-type compressor though an integrated dryer and pressure-controlled ballast tank. The fuel is stored in high-pressure high-purity hydrogen cylinders. The hydrogen control system reduces the pressure to a level appropriate for delivery to the fuel cell stack and then regulates the anode pressure to a desired level, which is typically set higher than the cathode pressure. Deionized water is used as a cooling medium in the test station to either heat or cool the stack using electric resistance heating and a heat exchanger with a controllable (on-off) fan. The thermostatic controller accepts a set-point and upper-lower thresholds for the power section outlet temperature of the coolant. An electric pump recirculates the coolant through a reservoir that is refilled. The coolant flow rate is controlled through a manual valve.

CONTROL VOLUME ANALYSIS

The control volume used for this analysis comprises the fuel cell stack and the humidification section, as indicated in Fig. 2. There are six mass streams crossing the boundary of the control volume: the coolant, the air, and the hydrogen flows entering and leaving the system. The dissipation of electric power is accounted for outside of the control volume.

[1]Standard liters per minute (slm) are the units used by the manufacturer. Although SI units are used in the rest of this article, the instrument specifications are quoted with the manufacturer's units.

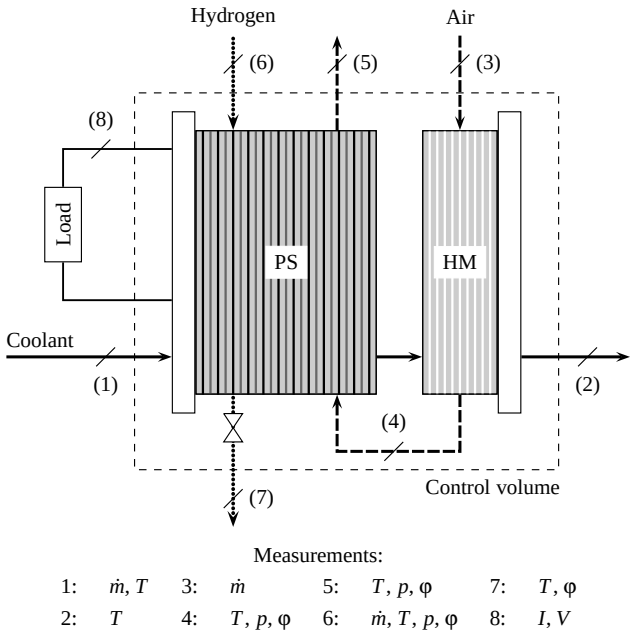

Figure 2. SCHEMATIC DIAGRAM OF THE FUEL CELL STACK WITH INTEGRATED HUMIDIFICATION SECTION AND MEASUREMENT LOCATIONS (1–8).

Energy Balance

In order to do a first-law control volume analysis, all contributions to the energy balance have to be determined. These are the sum of energy flows due to mass flows into and out of the control volume, the net rate of heat transfer, and of the net rate of work. Hence, for the control volume sketched in Fig. 2, the first law of thermodynamics is represented by the following differential equation,

$$\frac{\partial U}{\partial t} = \dot{H}_{Reac} + \Delta\dot{H}_{mAir}^{Excess} + \Delta\dot{H}_{mH_2}^{Purge} + \Delta\dot{H}_{H_2}^{Leak} + \Delta\dot{H}_{DI} - \dot{H}_{H_2O}^{EvapPS} - \dot{Q}_{Conv}^{B2Amb} - \dot{Q}_{Rad}^{B2Amb} - P_{El}\,. \quad (1)$$

This equation states that the rate of change of energy inside the control volume is equal to the sum of the reaction enthalpy rate, the enthalpy flow rates associated with the input and output mass streams, the evaporation enthalpy flow rate of water, the rate of heat transfer to the environment, and of the electric power. The kinetic and potential energy of the mass streams are small compared to the other contributions and may thus be neglected. In the following paragraphs, the contributions to the energy balance are discussed.

The reaction of hydrogen and oxygen to form liquid water is an exothermic chemical reaction. The energy of this reaction is calculated as the difference between the enthalpy of formation of the product and the enthalpies of formation of the reactants at the inlet and outlet, respectively,

$$\dot{H}_{Reac} = \dot{m}_{H_2}^{Reac}\left(h_f^0 + \Delta h\right)_{H_2} + \dot{m}_{O_2}^{Reac}\left(h_f^0 + \Delta h\right)_{O_2} - \dot{m}_{H_2O}^{Prod}\left(h_f^0 + \Delta h\right)_{H_2O\,(l)}\,, \quad (2)$$

where $\dot{m}$ denotes the mass flow rates of the substances, h_f^0 the mass specific enthalpy of formation with respect to a reference state, and Δh the mass specific enthalpy difference from the present state to the reference state. The mass flow rates of the reactants and the product are calculated from the measured electric current as

$$\dot{m}_{H_2}^{Reac} = M_{H_2} n_{Cells} \frac{1}{2F} I_{St} \quad (3)$$

$$\dot{m}_{O_2}^{Reac} = M_{O_2} n_{Cells} \frac{1}{4F} I_{St} \quad (4)$$

$$\dot{m}_{H_2O}^{Prod} = M_{H_2O} n_{Cells} \frac{1}{2F} I_{St}\,, \quad (5)$$

where M denotes the molecular masses in kg/mol, n_{Cells} is the number of fuel cells in the stack, and F the Faraday constant. For the enthalpy changes with respect to the reference state of the substances, constant specific heats are assumed,

$$\Delta h_{H_2} = C_{p0\,H_2}(T_{mH_2}^{PSIn} - T_0) \quad (6)$$

$$\Delta h_{O_2} = C_{p0\,O_2}(T_{mAir}^{HMIn} - T_0) \quad (7)$$

$$\Delta h_{H_2O} = C_{p\,H_2O(l)}(T_{mAir}^{PSOut} - T_0)\,, \quad (8)$$

where T_0 is the reference temperature. The air temperature at humidifier inlet, T_{mAir}^{HMIn}, has to be estimated because it is not measured. As indicated in Eqn. 8, the liquid product water is assumed to exit on the cathode side.

The reaction enthalpy term covers the reactant mass flows of the chemical reaction. However, these mass flows differ from the mass flows entering the system on the cathode as well as on the anode side. Specifically, the oxygen participating in the reaction is only one part of the moist air entering the system and a certain amount of hydrogen is typically used for purging the anode or is lost through leakage. The enthalpy changes of these gas mixtures which are only passing through the system therefore have to be calculated separately. In order to determine the enthalpy flows of the moist air, excluding the reacting oxygen, and of the purged moist hydrogen entering and leaving the system, the Dalton model is used. Hence, it is assumed that the enthalpy changes of the gas mixtures can be evaluated as the sum of the enthalpy changes of the water vapor and of the dry air or hydrogen, re-

spectively,

$$\Delta\dot{H}_{mAir}^{Excess} = \Delta\dot{H}_{Air}^{Excess} + \Delta\dot{H}_{H_2O}^{Excess} \quad (9)$$

$$\Delta\dot{H}_{mH_2}^{Purge} = \Delta\dot{H}_{H_2}^{Purge} + \Delta\dot{H}_{H_2O}^{Purge} . \quad (10)$$

For the gases, again, perfect gas behavior is assumed,

$$\Delta\dot{H}_{Air}^{Excess} = \dot{m}_{Air}^{Excess} C_{p0\,Air} \left(T_{mAir}^{HM\,In} - T_{mAir}^{PS\,Out}\right) \quad (11)$$

$$\Delta\dot{H}_{H_2O}^{Excess} = \dot{m}_{H_2O}^{mAir\,HM\,In} C_{p0\,H_2O(g)} \left(T_{mAir}^{HM\,In} - T_{mAir}^{PS\,Out}\right) , \quad (12)$$

and

$$\Delta\dot{H}_{H_2}^{Purge} = \dot{m}_{H_2}^{Purge} C_{p0\,H_2} \left(T_{mH_2}^{PS\,In} - T_{mH_2}^{PS\,Out}\right) \quad (13)$$

$$\Delta\dot{H}_{H_2O}^{Purge} = \dot{m}_{H_2O}^{mH_2\,PS\,In} C_{p0\,H_2O(g)} \left(T_{mH_2}^{PS\,In} - T_{mH_2}^{PS\,Out}\right) . \quad (14)$$

It is assumed that the specific heat of the excess air from which the reactant oxygen was removed equals the specific heat of air. The mass flow rate of excess air is the inlet mass flow rate minus the mass flow rate of oxygen consumed by the reaction,

$$\dot{m}_{Air}^{Excess} = \dot{m}_{Air}^{HM\,In} - \dot{m}_{O_2}^{Reac} . \quad (15)$$

The mass flow rate of purged hydrogen equals the inlet mass flow rate of hydrogen, minus the mass flow rate consumed by the reaction, minus the hydrogen lost by leakage,

$$\dot{m}_{H_2}^{Purge} = \dot{m}_{H_2}^{PS\,In} - \dot{m}_{H_2}^{Reac} - \dot{m}_{H_2}^{Leak} . \quad (16)$$

The mass flow rate of water vapor on the anode side can be calculated from the temperature, pressure, and relative humidity values at the inlet, as follows:

$$\dot{m}_{H_2O}^{mH_2\,PS\,In} = \frac{M_{H_2O}}{M_{H_2}} \dot{m}_{H_2}^{PS\,In} \frac{\varphi_{mH_2}^{PS\,In} p_{Sat}^{mH_2\,PS\,In}(T_{mH_2}^{PS\,In})}{p_{mH_2}^{PS\,In} - \varphi_{mH_2}^{PS\,In} p_{Sat}^{mH_2\,PS\,In}(T_{mH_2}^{PS\,In})} . \quad (17)$$

On the air side, the mass flow rate of water vapor entering the humidification section, $\dot{m}_{H_2O}^{mAir\,HM\,In}$, cannot be inferred through measurements and it is assumed negligible. This assumption is reasonable because the air flows through a dryer before it enters the mass air flow controller and the humidification section (location 3 in Fig. 2).

A certain amount of hydrogen is always lost through leakage (not marked in the schematic of Fig. 2). Even though the mass flow rate of leaking hydrogen is only known approximately, its enthalpy flow rate is considered within the energy balance,

$$\Delta\dot{H}_{H_2}^{Leak} = \dot{m}_{H_2}^{Leak} C_{p0\,H_2} \left(T_{mH_2}^{PS\,In} - \frac{1}{2}(T_{mH_2}^{PS\,In} + T_{mH_2}^{PS\,Out})\right) . \quad (18)$$

The mass flow rate of leaking hydrogen, $\dot{m}_{H_2}^{Leak}$, is estimated and its temperature is assumed to be the mean of the inlet and outlet temperatures.

The coolant enters the system at the power section inlet, partially evaporates into the air stream inside the humidification section, and exits the system as liquid fraction into the coolant loop at the humidifier outlet and as vapor fraction at the cathode outlet. Hence, the enthalpy difference of the coolant equals the enthalpy of the coolant at the power section inlet minus the enthalpy of the coolant at the humidifier outlet, minus the enthalpy of the vaporized coolant at the cathode outlet,

$$\begin{aligned}\Delta\dot{H}_{DI} = {} & \dot{m}_{DI}^{PS} C_{p\,H_2O(l)} (T_{DI}^{PS\,In} - T_{DI}^{HM\,Out}) \\ & + \dot{m}_{H_2O}^{Evap\,HM} \big(C_{p0\,H_2O(g)} (T_{DI}^{HM\,Out} - T_{mAir}^{PS\,Out}) \\ & - (h_{fg})_{H_2O} (T_{DI}^{HM\,Out})\big) . \end{aligned} \quad (19)$$

The specific evaporation enthalpy, h_{fg}, is a function of the respective temperature. Here, it is assumed that the coolant evaporates at the outlet temperature, $T_{DI}^{HM\,Out}$. The mass flow rate of the coolant evaporated, $\dot{m}_{H_2O}^{Evap\,HM}$, could be determined as the difference of the measured coolant flowing into and out of the system. But as the vapor fraction could be negligibly small compared to the total coolant mass flow rate, this value would be inaccurate. Instead, the water contents of the gas stream at the humidifier inlet and outlet are used to calculate the mass of coolant that has evaporated inside the humidification section,

$$\dot{m}_{H_2O}^{Evap\,HM} = \dot{m}_{H_2O}^{mAir\,HM\,Out} - \dot{m}_{H_2O}^{mAir\,HM\,In} . \quad (20)$$

At the humidifier inlet, as mentioned above, the water mass flow rate has been assumed to be equal to zero. At the humidifier outlet it is calculated as a function of the temperature, pressure, and relative humidity measurements,

$$\begin{aligned}\dot{m}_{H_2O}^{mAir\,HM\,Out} = {} & \frac{M_{H_2O}}{M_{Air}} \dot{m}_{Air}^{HM\,In} \\ & \cdot \frac{\varphi_{mAir}^{HM\,Out} p_{Sat}^{mAir\,HM\,Out}(T_{mAir}^{HM\,Out})}{p_{mAir}^{HM\,Out} - \varphi_{mAir}^{HM\,Out} p_{Sat}^{mAir\,HM\,Out}(T_{mAir}^{HM\,Out})} . \end{aligned} \quad (21)$$

In order to determine the enthalpy difference of the chemical reaction, the product water is assumed to be in liquid form

(Eqn. 2), and in Eqns. 12 and 14 the vapor carried by the moist air and the moist hydrogen is assumed to pass the system without any change of its state of aggregation. A change in the state of aggregation of the water is coupled to a change in its enthalpy: the evaporation of water removes energy from the system, whereas the condensation of vapor releases energy. By determining the difference of water vapor entering and leaving the power section the additional enthalpy flow due to evaporation (or condensation) can be calculated,

$$\begin{aligned}\dot{H}_{H_2O}^{Evap\,PS} = &\left(\dot{m}_{H_2O}^{mAir\,PSOut} - \dot{m}_{H_2O}^{mAir\,PSIn}\right)\cdot(h_{fg})_{H_2O}(T_{mAir}^{PSOut}) \\ &+ \left(\dot{m}_{H_2O}^{mH_2\,PSOut} - \dot{m}_{H_2O}^{mH_2\,PSIn}\right) \\ &\cdot\left(C_{pH_2O(l)}(T_{mAir}^{PSOut} - T_{mH_2}^{PSOut}) + (h_{fg})_{H_2O}(T_{mH_2}^{PSOut})\right),\end{aligned} \tag{22}$$

with

$$\begin{aligned}\dot{m}_{H_2O}^{mAir\,PSOut} = &\frac{M_{H_2O}}{M_{Air}}\,\dot{m}_{Air}^{Excess} \\ &\cdot\frac{\varphi_{mAir}^{PSOut}\,p_{Sat}^{mAir\,PSOut}(T_{mAir}^{PSOut})}{p_{mAir}^{PSOut} - \varphi_{mAir}^{PSOut}\,p_{Sat}^{mAir\,PSOut}(T_{mAir}^{PSOut})}\end{aligned} \tag{23}$$

$$\begin{aligned}\dot{m}_{H_2O}^{mH_2\,PSOut} = &\frac{M_{H_2O}}{M_{H_2}}\,\dot{m}_{H_2}^{Purge} \\ &\cdot\frac{\varphi_{mH_2}^{PSOut}\,p_{Sat}^{mH_2\,PSOut}(T_{mH_2}^{PSOut})}{p_{mH_2}^{PSOut} - \varphi_{mH_2}^{PSOut}\,p_{Sat}^{mH_2\,PSOut}(T_{mH_2}^{PSOut})},\end{aligned} \tag{24}$$

and $\dot{m}_{H_2O}^{mH_2\,PSIn}$ and $\dot{m}_{H_2O}^{mAir\,PSIn} = m_{H_2O}^{mAir\,HMOut}$ defined further above (Eqns. 17 and 21). As the product water is assumed to exit on the cathode side, the enthalpy difference between cathode and anode has to be added in Eqn. 22 for the water evaporated on the anode side. In Eqn. 23, M_{Air} is used for the molecular mass of the excess air. The pressure at the anode outlet, $p_{mH_2}^{PSOut}$, is not measured but can be safely approximated as the ambient pressure. The specific evaporation enthalpies, h_{fg}, are functions of the respective temperatures T_{mAir}^{PSOut} and $T_{mH_2}^{PSOut}$.

As the fuel cell system body has a different temperature than its surroundings, heat is lost through its surface. The heat transfer to the surrounding area consists of a convective and a radiative heat flow,

$$\dot{Q}_{Conv}^{B2Amb} = (hA)_{B2Amb}\,(T_{Syst} - T_{Amb}) \tag{25}$$

$$\dot{Q}_{Rad}^{B2Amb} = \varepsilon\sigma A_{B2Amb}\left(T_{Syst}^4 - T_{Amb}^4\right). \tag{26}$$

The convective heat transfer coefficient, h_{B2Amb}, is a function of the medium properties, the flow, and the geometry. It was determined using standard heat transfer correlations for natural convection [5]. As the coefficient differs for horizontal and vertical surfaces, the surface area was partitioned and the coefficients for the vertical area elements, the horizontal upper and the horizontal lower areas were calculated separately. The overall heat transfer coefficient was then calculated as the area-weighted sum of the individual coefficients. A rough estimation is used for the emissivity, ε, of the body. The parameter A_{B2Amb} denotes the outer surface area of the body, σ is the Stefan-Boltzmann constant, T_{Amb} represents the temperature of the environment, and T_{Syst} is the system temperature.

Depending on the amount of current drawn and other influencing quantities, the fuel cell stack produces an output voltage. The electric power delivered by the system equals the product of this stack voltage, V_{St}, and the current drawn, I_{St},

$$P_{El} = V_{St}\,I_{St}\,. \tag{27}$$

Experimental Results for Energy Balance. The energy balance is evaluated with a set of measurement data acquired on the test bench. The measurement data results from an experimental run during which the fuel cell system was operated at different power levels and with different coolant inlet conditions. By changing the power level and varying the coolant inlet conditions, the system dynamics are excited. In Fig. 3 all sensor data is plotted against time. In subplot one, the power output is plotted instead of the electric current. The electric power drawn from the system changes between about 350 W and 900 W. The same subplot shows the resulting stack voltage. Subplot two shows the coolant mass flow rate. The coolant mass flow rate varies between 0.6 kg/min and 1.4 kg/min. The coolant inlet temperature, which is a function of the heat exchanger fan operation, fluctuates within 40 °C and 55 °C. The coolant inlet and outlet temperatures are depicted in subplot three. Subplot four shows the controlled air and hydrogen mass flow rates. The remaining six subplots show the properties of the air and the hydrogen at power section inlet and outlet, respectively. These are the temperatures, pressures, and relative humidities. Note that the pressure at the anode outlet is not measured. There are no measurements of the temperature and of the humidity of the air stream at the humidifier inlet, nor of the mass flow rate of leaking hydrogen, either. These non-measured quantities are estimated as follows:

$$T_{mAir}^{HMIn} = 20\,^{\circ}\mathrm{C}$$
$$\dot{m}_{H_2O}^{mAir\,HMIn} = 0\,\mathrm{g/s}$$
$$p_{mH_2}^{PSOut} = 1.013\,\mathrm{bar}$$
$$\dot{m}_{H_2}^{Leak} = 5.6{\cdot}10^{-4}\,\mathrm{g/s}.$$

The ambient temperature was set constant to

$$T_{Amb} = 25\,^{\circ}\mathrm{C}.$$

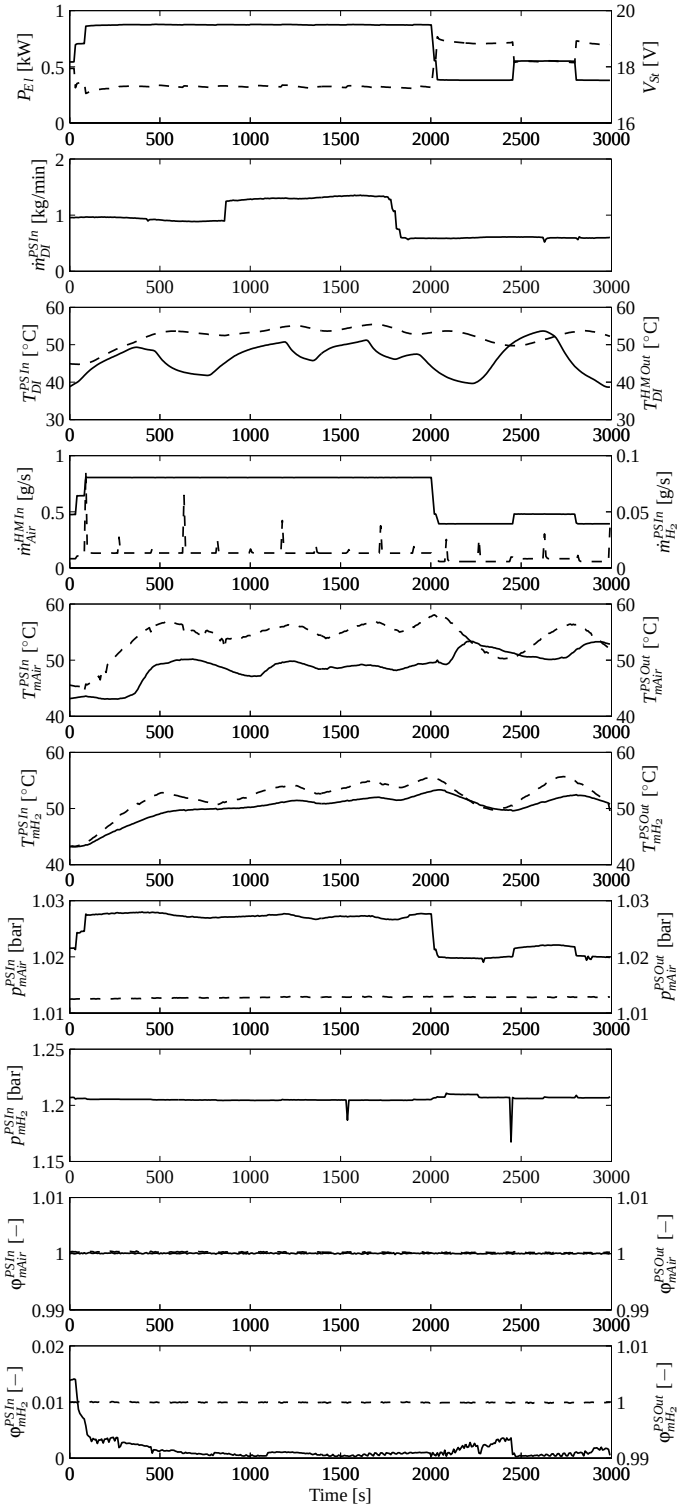

Figure 3. EXPERIMENTAL DATA USED FOR EVALUATION OF THE CONTROL VOLUME ANALYSIS AND FOR MODEL PARAMETER IDENTIFICATION (LEFT AXIS: SOLID LINE, RIGHT AXIS: DASHED LINE).

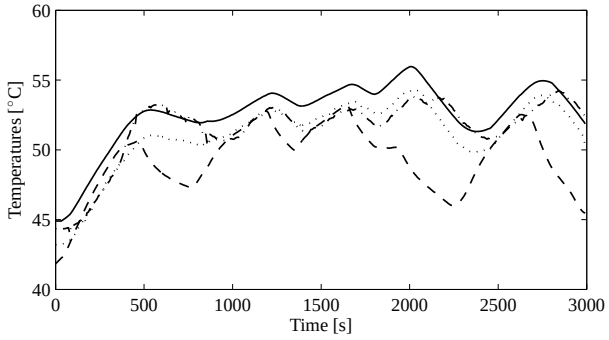

Figure 4. COMPARISON OF TEMPERATURE CURVES FROM THE ENERGY BALANCE ANALYSIS: CALCULATED SYSTEM TEMPERATURE (–), COOLANT TEMPERATURE (- -), CATHODE TEMPERATURE (·-), ANODE TEMPERATURE (··).

If all the measurement data, together with the estimations of the non-measured quantities stated above, are inserted into Eqns. 2–27 and eventually into Eqn. 1, a nonlinear differential equation results,

$$m_{Syst}\, C_{Syst} \frac{\partial T_{Syst}}{\partial t} = f(T_{Syst}, t), \tag{28}$$

where $m_{Syst}\, C_{Syst}$ is the thermal capacity of the system. By integrating this differential equation, the temperature of the fuel cell system can be calculated as a function of time. As no measurement of the system temperature exists the calculated system temperature is compared with the available temperature measurements to check the assumptions and calculations in the control volume analysis. In Fig. 4 the calculated system temperature curve is plotted, together with the coolant temperature, the cathode and the anode temperature, which are supposed to be the average of the measured system input and output temperatures of the respective mass streams. The system temperature was initialized with the coolant outlet temperature. It can clearly be seen that the calculated system temperature is close to the other temperatures and exhibits reasonable transient behavior. Since Eqn. 28 is an open integrator except for the influence of the heat losses to the ambient, small deviations in the energy balance would result in a divergence of the calculated system temperature. The general agreement of the measured and calculated temperatures indicates that the experimental setup is free of significant measuring errors and that the assumptions for the non-measured quantities are reasonable. A detailed sensitivity analysis is provided a subsequent section.

The energy balance reveals the influence of the different energy flows on the thermal dynamics of the system. In order to gain more insight, it is useful to analyze the individual contributions to the change in internal energy of the fuel cell system.

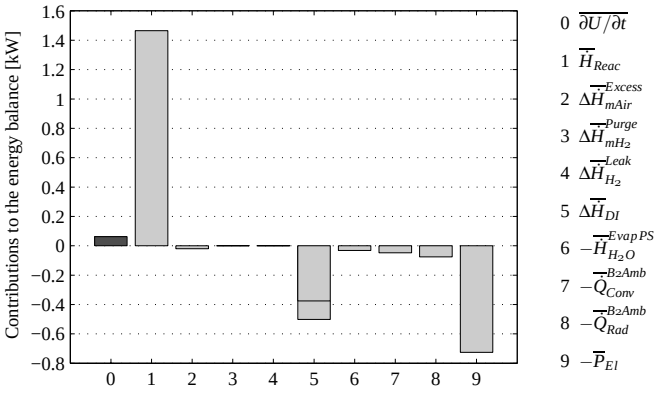

Figure 5. CHANGE (0) AND CONTRIBUTIONS TO THE CHANGE (1–9) IN INTERNAL ENERGY OF THE FUEL CELL SYSTEM.

Therefore, every term of Eqn. 1 is calculated separately. To facilitate the comparison all contributions are averaged over the duration of the experiment shown in Fig. 3. In Fig. 5 the mean contributions to the change in internal energy of the fuel cell system are depicted in a bar graph. For the experiment investigated, the average energy flow contributed by the chemical reaction (bar 1) is 1460 W. About half of it is usable electric power (bar 9), the remainder is waste heat. The main part (51%) of the waste heat is carried away by the coolant loop (bar 5, bigger part), another 17% as latent heat of the evaporated coolant (bar 5, smaller part). The heat losses to the environment (bars 7 and 8) amount to 17% of the total waste heat, whereas both the convective and the radiative losses are of a similar magnitude. A fraction of 8.4% of the waste heat is used to heat up the system (bar 0). The remaining waste heat (7.0%) is used to evaporate product water (bar 6) and heat up the gases (bars 2, 3, and 4). The values of all averaged energy flows are listed in Tab. 1 as absolute values and in comparison to the average reaction enthalpy flow, $\overline{\dot{H}}_{Reac}$. By far the smallest contributions to the energy balance stem from the leakage and the purging. Despite its higher specific heat, the enthalpy difference of the purged moist hydrogen is between two and three orders of magnitude smaller than that of the moist excess air. This is mainly caused by the significant difference in the mass flow rates and the smaller temperature change of the anode flow between inlet and outlet. The averaged energy flows are indicated with a bar ($\overline{\cdot}$) in Fig. 5 and Tab. 1.

Water (H_2O) Mass Balance

A water mass balance of the gas channels is developed similarly to the energy balance presented before. If no storage of water inside the system is assumed, the H_2O mass balance of the gas channels is represented by the following equation,

$$0 = \dot{m}_{H_2O}^{Prod} + \dot{m}_{H_2O}^{EvapHM} + \dot{m}_{H_2O}^{mAirHMIn} + \dot{m}_{H_2O}^{mH_2PSIn} - \dot{m}_{H_2O}^{mAirPSOut} - \dot{m}_{H_2O}^{mH_2PSOut} - \dot{m}_{H_2O}^{LiqOut}, \quad (29)$$

stating that the rate of water produced within the system plus the rate of water entering the system equals the mass flow rate of outgoing water. The first six mass flow rates of Eqn. 29 are determined as defined in the energy balance section (compare Eqns. 5, 17, 20, 21, 23, and 24, $\dot{m}_{H_2O}^{mAirHMIn}$ is guessed). The mass flow rate of water exiting the gas channels in liquid form, $\dot{m}_{H_2O}^{LiqOut}$, is then determined to fulfill the mass balance.

Table 1. AVERAGED FIRST-LAW ENERGY FLOWS OF THE FUEL CELL SYSTEM.

Term	Absolute value [W]	Fraction of $\overline{\dot{H}}_{Reac}$ [%]
$\overline{\partial U/\partial t}$	62.1	4.2
$\overline{\dot{H}}_{Reac}$	1460	100
$\Delta\overline{\dot{H}}_{mAir}^{Excess}$	20.3	1.4
$\Delta\overline{\dot{H}}_{mH_2}^{Purge}$	0.0235	0.0016
$\Delta\overline{\dot{H}}_{H_2}^{Leak}$	0.00760	0.00052
$\Delta\overline{\dot{H}}_{DI}$	501	34
$\overline{\dot{H}}_{H_2O}^{EvapPS}$	31.7	2.2
$\overline{\dot{Q}}_{Conv}^{B2Amb}$	47.4	3.2
$\overline{\dot{Q}}_{Rad}^{B2Amb}$	75.6	5.2
$\overline{P}_{El}$	726	50

Experimental Results for Water Mass Balance. The contributions to the H_2O mass balance of Eqn. 29 are calculated for the experimental data shown in Fig. 3 and averaged over experiment duration. The averaged mass flow rates are depicted in Fig. 6 as a bar graph. For an electric output power of about 730 W a water mass flow rate of approximately 0.09 g/s is produced (bar 1). The amount of water produced by the chemical reaction is proportional to the electric current. The product water exits the system as liquid and also as vapor, as it is partially evaporated inside the fuel cells. In this experiment, about 86% of the product water exit the system in liquid form (bar 7), the remaining 14% are evaporated. The fraction of product water that is evaporated is calculated as the difference of the total product water and the water exiting the system in liquid form (or equivalent as the difference of the water vapor leaving and entering the power section). About 0.05 g of coolant are evaporated per sec-

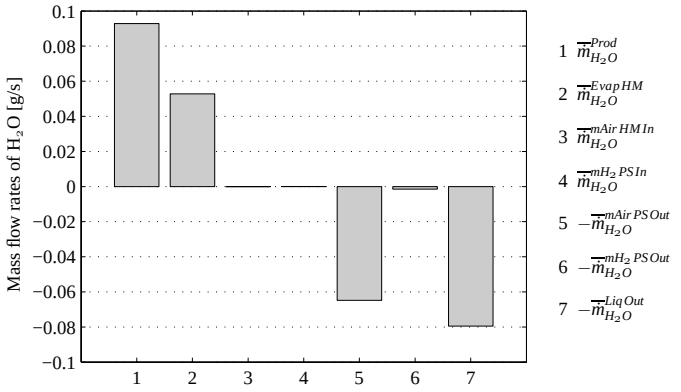

Figure 6. CONTRIBUTIONS TO THE H_2O MASS BALANCE FOR THE GAS FLOW CHANNELS.

ond (bar 2), which are 0.3% of the total coolant mass flow rate of approximately 15 g/s. As the supplied gases are dry, the humidity at the inlet[2] is small (bars 3 and 4). At the outlet, the mass of the water carried by the air is much larger than that carried by the hydrogen (bars 5 and 6), despite the higher storage capacity of water mass per unit mass of hydrogen. The effect is mainly due to the significant difference in the mass flow rate of the excess air and the mass flow rate of the purged hydrogen ($\overline{\dot{m}}^{Excess}_{Air} = 0.6$ g/s, $\overline{\dot{m}}^{Purge}_{H_2} = 0.001$ g/s).

Sensitivity Analysis

The equations of the energy balance contain measurement data values, physical constants, material properties, system parameters, and estimated signals. However, the measured signals are subject to sensor mis-calibration and the system parameters as well as the four estimated signals are subject to modeling errors. In order to quantify the influence of uncertainty in these quantities, a sensitivity analysis was performed. Following Eqn. 28, the underlying equation of the sensitivity analysis was defined as

$$\frac{\partial U}{\partial t} + \Delta\left(\frac{\partial U}{\partial t}\right)_i = f(\xi_i + \Delta\xi_i)\,, \tag{30}$$

where

$$\frac{\partial U}{\partial t} = f(\xi)\,, \quad \xi:\ \text{Parameters, Signals}\,. \tag{31}$$

In the sensitivity analysis the impact, $\Delta(\partial U/\partial t)_i$, of signal offsets or of parameter deviations, $\Delta\xi_i$, from their nominal values, ξ_i, on the change in internal energy of the system, $\partial U/\partial t$, is investigated. The nominal conditions were set to the average values of the experiment shown in Fig. 3 and to the estimated values stated in the energy balance section. This corresponds to typical operating conditions with an electric output power of approximately 730 W. The offsets and deviations, $\Delta\xi_i$, were chosen to reflect the uncertainty of the corresponding quantity, which is the calibration and sensor tolerance for the measurement signals and a judicious guess of the uncertainty for the estimated signals and the system parameters.

Table 2. RESULTS OF THE SENSITIVITY ANALYSIS.

Quantity	Nom. value	Deviation	Sensitivities	
	ξ_i	$\Delta\xi_i$	S_i [W]	s_i [%]
T^{PSIn}_{DI}	319 K	1 K	64	8.7
$\dot{m}^{PSIn}_{DI}$	0.0153 kg/min	0.02 kg/min	-8.4	-1.1
T^{HMIn}_{mAir}	293 K	5 K	3.4	0.46
$\dot{m}^{mAir\,HM\,In}_{H_2O}$	0 g/s	$1.2\cdot10^{-3}$ g/s	2.8	0.38
$p^{PSOut}_{mH_2}$	$1.01\cdot10^5$ Pa	5000 Pa	0.18	0.025
$\dot{m}^{Leak}_{H_2}$	$5.6\cdot10^{-4}$ g/s	$2.8\cdot10^{-4}$ g/s	0.93	0.13
h_{B2Amb}	3.9	1 W/(m^{2}K)	-12	-1.7
ε	0.9	0.1	-8.4	-1.1

Table 2 shows the results of the sensitivity analysis for a selection of sensor signals, the estimated signals, and for two system parameters. The sensitivities are listed as absolut values, S_i, and as fractions, s_i, of the waste heat of the chemical reaction,

$$S_i := \Delta\left(\frac{\partial U}{\partial t}\right)_i\,, \quad s_i := \frac{S_i}{\overline{\dot{H}}_{Reac} - \overline{P}_{El}}\,. \tag{32}$$

From all sensor signals, the sensor signal with the highest impact on the energy balance is the temperature of the coolant at the power section inlet, T^{PSIn}_{DI}. A sensor or calibration error of 1 K results in an error of 64 W in the energy balance. This error merits special attention since it corresponds to 8.7% of the total waste heat of the chemical reaction. An assumed error of 0.02 kg/min in the highly accurate coolant mass flow measurement leads to an offset of -8.4 W in the energy balance. The sensitivities of the estimated signals T^{HMIn}_{mAir}, $\dot{m}^{mAir\,HM\,In}_{H_2O}$, $p^{PSOut}_{mH_2}$, and $\dot{m}^{Leak}_{H_2}$ reveal that the uncertainty in these quantities does not affect much the energy balance. For the temperature a deviation of 5 K was chosen and the deviation of the mass of vapor in the (dried) inlet air stream was chosen to be 2% of the vapor mass in the outlet air stream. The deviation of the anode outlet pressure was set to 5000 Pa, which are about 5% of the nominal value, and the deviation of the leakage mass flow rate was set to

[2]Humidifier inlet for the air stream, power section inlet for the hydrogen stream.

50% of its nominal value. The impacts on the energy balance are 3.4 W, 2.8 W, 0.18 W, and 0.93 W, respectively. A change of 1 W/(m^{2}K) in the heat transfer coefficient, h_{B2Amb}, results in an offset of -12 W in the energy balance, whereas an uncertainty of 0.1 in the emissivity, ε, corresponds to an offset of -8.4 W.

The sensitivity analysis allows two main conclusions. First, the results demonstrate that accurate temperature sensors and sensor calibration are of inevitable importance for the control volume analysis of low-temperature systems such as PEM fuel cells. Second, it has to be stressed that for identifying system parameters, such as heat transfer coefficients, the measurements have to be very accurate. From the results in Tab. 2 it is apparent that an error of only 1 K in the coolant inlet measurement would lead to an approximate error of 5 W/(m^{2}K) in the convective heat transfer coefficient. This result is alarming, as the 5 W/(m^{2}K) are 130% of its nominal value. It is noteworthy that the authors in [1] document a significant disagreement in the convective heat transfer coefficient derived experimentally and values expected from standard natural convection.

By evaluating Eqn. 30 from left to right, the sensitivity analysis helps to determine the required accuracy of every sensor. Starting with a tolerated uncertainty, $\Delta(\partial U/\partial t)$, the sensor tolerances, $\Delta\xi_i$, can be calculated.

CONTROL-ORIENTED MODEL

A lumped-parameter approach is introduced for the modeling of the fuel cell system. Particularly, the spatial inhomogeneities in the stack temperature and in the heat transfer coefficients are ignored. Complex phenomena such as membrane humidification or water transport perpendicular to the membrane are neglected as well.

As a first step when developing a control-oriented model for a physical system, the system boundaries have to be defined, i.e. the input and output signals have to be stated. Next, all relevant dynamics of the system have to be identified, where relevant dynamics are dynamics which exhibit similar transients as the system outputs. Fast dynamics can be modeled statically, slow dynamics as constants. For the fuel cell system thermal model the variable of main interest is the bulk system temperature. The time constant of this dynamic can be estimated by analyzing Eqn. 1. Depending on the operating conditions a time constant of about 10^2 s is calculated. The time constants of the electrochemistry, of the RC-element of the electrode/membrane system, and of the hydrogen and air manifold dynamics are several orders of magnitude faster. In [6] these time constants are estimated to be in the order of magnitude of 10^{-9} s for the electrochemistry and the RC-element and of 10^{-1} s for the manifold dynamics, respectively. As a consequence, these dynamics can be modeled as quasi-static processes. Rough calculations for the dynamics of the coolant inside the power section and the coolant inside the humidifier reveal time constants of about the order of magnitude of 10 s.

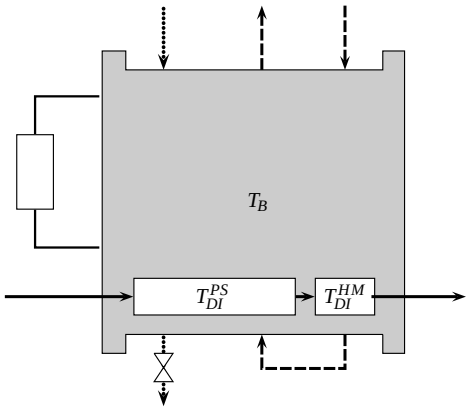

Figure 7. DYNAMIC SUBSYSTEMS OF THE FUEL CELL SYSTEM MODEL WITH STATE VARIABLES T_B, T_{DI}^{PS}, AND T_{DI}^{HM}.

Based on this analysis the fuel cell system was modeled to consist of three dynamic subsystems: the body of the fuel cell system, the coolant inside the power section and the coolant inside the humidifier. The corresponding state variables are the bulk fuel cell system temperature, the mean temperature of the coolant mass inside the power section, and the mean temperature of the coolant mass inside the humidification section. All other dynamics are considered to be fast and thus modeled quasi-statically. A schematic overview of the subsystems is given in Fig. 7.

In order to find the governing differential equations of the system dynamics a control volume approach is applied to each subsystem. Thus, the energy balance of Eqn. 1 splits into three differential equations, one for each subsystem. These equations are coupled through energy flows connecting the subsystems. A causality and input-output diagram of the fuel cell system model is depicted in Fig. 8. Based on the current demand, I_{St}, and the coolant inlet conditions ,$T_{DI}^{PS\,In}$ and $\dot{m}_{DI}^{PS\,In}$, the model predicts the system temperature, T_B, the coolant outlet temperature, $T_{DI}^{HM\,Out}$, and the stack voltage, V_{St}. Hence, the model exhibits three input and three output signals.

In the following, the differential equations of the subsystems are stated and all energy flows crossing the boundaries and those interacting between the subsystems are modeled. Note that this modeling effort is more extensive than the heat balance analysis presented in the previous section due to two reasons: first, there are three control volumes instead of one, and second, the measurement signals, excluding the three remaining input signals, have to be modeled as well. However, the results from the previous section allows to define the relevant contributions to the thermal dynamics.

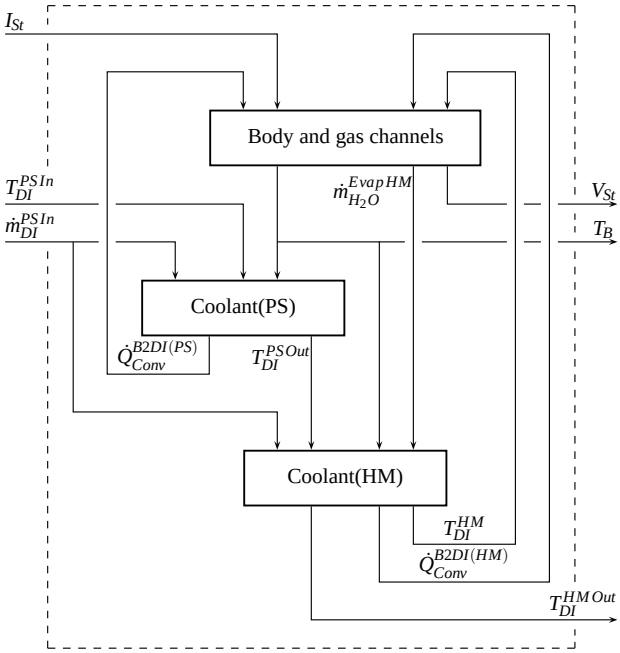

Figure 8. CAUSALITY DIAGRAM OF THE DYNAMIC FUEL CELL SYSTEM LUMPED-PARAMETER MODEL WITH INPUT SIGNALS $I_{St}, T_{DI}^{PS\,In}, \dot{m}_{DI}^{PS\,In}$ AND OUTPUT SIGNALS $V_{St}, T_B, T_{DI}^{HM\,Out}$.

Body and Gas Channels

Applying a control volume analysis to the fuel cell system body yields the following energy balance differential equation,

$$m_B C_B \frac{\partial T_B}{\partial t} = \dot{H}_{Reac} + \Delta\dot{H}_{mAir}^{Excess} - \dot{Q}_{Conv}^{B2DI(PS)} - \dot{Q}_{Conv}^{B2DI(HM)} - \dot{H}_{H_2O}^{Evap\,PS} - \dot{Q}_{Conv}^{B2Amb} - \dot{Q}_{Rad}^{B2Amb} - P_{El}\,. \quad (33)$$

Below, this equation is explained and also compared with the energy balance of the entire system (Eqn. 1). As the thermal capacity of the fuel cell system body, $m_B C_B$, differs from the thermal capacity of the total system, the index B is introduced here. The reaction enthalpy, $\dot{H}_{Reac}$, is calculated according to Eqn. 2. In order to calculate the enthalpy difference of the reactants and the product from the present state to the reference state, the respective inlet and outlet temperatures have to be modeled. The calculation of the enthalpy difference of the moist excess air, $\Delta\dot{H}_{mAir}^{Excess}$, needs additionally the mass flow rate of dry air and the mass flow rate of vapor carried by the excess air at the inlet to be known. As apparent from Fig. 5 and Tab. 1 and as discussed earlier, the enthalpy flows of the leaking hydrogen and of the purged moist hydrogen are small compared to the other enthalpy flows, and, as a consequence, can be neglected. The energy carried away by the coolant is modeled as two convective heat flows: the heat flow from the body to the coolant inside the power section, $\dot{Q}_{Conv}^{B2DI(PS)}$, and the heat flow to the coolant inside the humidification section, $\dot{Q}_{Conv}^{B2DI(HM)}$. The energy removed by the evaporation of coolant is accounted for in the humidifier subsystem. In order to calculate the evaporation enthalpy inside the power section, $\dot{H}_{H_2O}^{Evap\,PS}$, a H_2O mass balance has to be implemented. The mass flow rate of the evaporated product water is calculated as the difference between the inflowing and the effused mass flow rate of vapor. The water contents of the air stream at the power section inlet and the power section outlet are determined from the respective temperature, pressure and relative humidity values. The vapor on the anode side is neglected, as the mass flow rate is comparably small (compare Fig. 6, mass flow rates 4 and 6). The remaining terms of Eqn. 33 coincide with the corresponding terms of Eqn. 1. In order to predict the voltage output of the fuel cells, a quasi-static electrochemical model was implemented. In previous studies, for example [7–9], different voltage models have been developed. In the present study, the model of [9] was adopted,

$$V_{Cell} = E - \nu_{Act} - \nu_{Ohm} - \nu_{Conc}\,. \quad (34)$$

The cell voltage is written as the thermodynamic potential E minus the activation overvoltage, ν_{Act}, minus the ohmic overvoltage, ν_{Ohm}, minus the concentration overvoltage, ν_{Conc}, where

$$E = E(T_B, p_{H_2}^{PS}, p_{O_2}^{PS}) \quad (35)$$

$$\nu_{Act} = \nu_{Act}(i_{St}, p_{mAir}^{PS}, T_{mAir}^{PS}, p_{O_2}^{PS}) \quad (36)$$

$$\nu_{Ohm} = \nu_{Ohm}(i_{St}, T_B, \lambda_m) \quad (37)$$

$$\nu_{Conc} = \nu_{Conc}(i_{St}, T_B, p_{O_2}^{PS}, T_{mAir}^{PS})\,. \quad (38)$$

The parameter λ_m denotes the membrane water content (which is assumed constant), i_{St} is the current density, which equals stack current per active area, $p_{H_2}^{PS}$ and $p_{O_2}^{PS}$ are the partial pressures of hydrogen and oxygen, respectively. The partial pressures can be calculated from the total pressures, the temperatures and the relative humidities on the anode and cathode side, respectively. The overvoltages ν_{Act}, ν_{Ohm}, and ν_{Conc} are expressed as a combination of physical and empirical relationships. The empirical parameters were determined using nonlinear regression on fuel cell polarization data. The stack voltage is defined as the sum of all individual cell voltages,

$$V_{St} = n_{Cells} V_{Cell}\,. \quad (39)$$

In order to provide temperatures, pressures, relative humidities and mass flow rates, a quasi-static model of the gas channels is implemented. The pressure drop over the cathode channel is

described by a linearized nozzle with nozzle constant k_p,

$$p_{mAir}^{PSIn} = p_{mAir}^{PSOut} + \frac{\dot{m}_{Air}^{HMIn}}{k_p}\,, \tag{40}$$

where the pressure at the cathode outlet, p_{mAir}^{PSOut}, is set to ambient pressure. Assuming the gas supply system to be perfectly controlled, the mass flow rate of dry air entering the system, $\dot{m}_{Air}^{HMIn}$, was modeled proportional to the mass flow rate of reactant oxygen,

$$\dot{m}_{Air}^{HMIn} = \lambda_{Air} \frac{1}{0.21} \frac{M_{Air}}{M_{O_2}} \dot{m}_{O_2}^{Reac}\,. \tag{41}$$

The air excess ratio λ_{Air} is considered a known operating parameter (typically within the range $2.0-3.5$) that is perfectly controlled through the reactant control subsystem. The constant k_p can be determined by parameter identification. The anode pressure can be determined though the cathode pressure,

$$p_{mH_2}^{PS} = p_{mAir}^{PS} + \Delta p_{AnCa}\,, \tag{42}$$

since the goal of the hydrogen control subsystem is to supply the necessary hydrogen while maintaining a constant pressure drop over the membrane. Again, a perfectly-controlled gas supply system is presumed here. The cathode pressure, p_{mAir}^{PS}, is calculated as the average of the cathode inlet and outlet pressures. The temperatures of both gas streams are assumed to be known at the inlet. The values are selected based on the ambient conditions, but their selection is not very critical as can be shown. Hence, they are included into the model as non-varying input parameters. The air temperature at the humidifier outlet (or the power section inlet) is defined to be equal to the temperature of the coolant inside the humidification section. In order to calculate the air temperature at the power section outlet, the following approach is made,

$$T_{mAir}^{PSOut} = 2 \cdot T_{mAir}^{PS} - T_{mAir}^{PSIn}\,, \tag{43}$$

where

$$T_{mAir}^{PS} = T_B - \frac{\dot{H}_{Reac} - P_{El}}{k_T}\,. \tag{44}$$

Here, it is assumed that the temperature difference between the body of the fuel cell and the cathode air is proportional to the total waste heat of the reaction. The constant of proportionality is defined as $1/k_T$, which can be determined experimentally. This simple model yields satisfactory agreement with measurement data. The temperature of the hydrogen in the anode is calculated as the mean value of the hydrogen inlet and outlet temperatures, with the temperature of the hydrogen at the outlet assumed to be equal to the temperature of the system body. This assumption is justified because of the small mass flow rate. The water content of the supplied air at the humidifier inlet is directly assigned as an input parameter. At the humidifier outlet (or the power section inlet, respectively), the air stream is supposed to be saturated. The relative humidity of the air stream at the power section outlet is also set to one, provided that enough water enters the system. Otherwise, it is assumed that all water is evaporated, and the relative humidity is modified accordingly. The relative humidity of the hydrogen is directly assigned. It is set to 0.5, as the hydrogen enters the system almost dry and leaves the system saturated, as it is apparent from the measurement data shown in Fig. 3.

Coolant Mass of Power Section. The governing differential equation for the energy balance of the coolant inside the power section is given as

$$m_{DI(PS)} C_{DI} \frac{\partial T_{DI}^{PS}}{\partial t} = \Delta \dot{H}_{DI}^{PS} + \dot{Q}_{Conv}^{B2DI(PS)}\,. \tag{45}$$

The change in the lumped coolant temperature is a function of the enthalpy difference of the coolant flow, $\Delta \dot{H}_{DI}^{PS}$, and of the convective heat transfer rate, $\dot{Q}_{Conv}^{B2DI(PS)}$. The enthalpy difference of the coolant flow depends on the coolant mass flow rate and on the coolant temperatures at the power section inlet and outlet. The coolant mass flow rate and the inlet temperature are input signals and thus given. At the outlet, the temperature is calculated as a function of the lumped temperature as

$$T_{DI}^{PSOut} = 2 \cdot T_{DI}^{PS} - T_{DI}^{PSIn}\,. \tag{46}$$

The convective heat transfer rate from the body to the coolant inside the power section is modeled according to Newton's law of cooling as

$$\dot{Q}_{Conv}^{B2DI(PS)} = (hA)_{B2DI(PS)} \cdot (T_B - T_{DI}^{PS})\,, \tag{47}$$

where $A_{B2DI(PS)}$ is the heat transfer area and $h_{B2DI(PS)}$ the heat transfer coefficient. The heat transfer coefficient is a function of the geometry, the medium properties, and the flow conditions. The geometry is constant, and for small temperature variations also the medium properties are, whereas the flow conditions can change. In formal analogy to heat transfer correlations for forced

convection, the following simple approach is used to define the heat transfer coefficient as a function of the mass flow rate of the coolant:

$$h_{B2DI(PS)} = K_h \cdot (\dot{m}_{DI}^{PS})^{\delta_h} . \tag{48}$$

The coefficients K_h and δ_h have to be determined experimentally.

Coolant Mass of Humidification Section

The energy balance of the coolant inside the humidification section is similar to the energy balance of the power section (Eqn. 45),

$$m_{DI(HM)}\, C_{DI} \frac{\partial T_{DI}^{HM}}{\partial t} = \Delta \dot{H}_{DI}^{HM} + \dot{Q}_{Conv}^{B2DI(HM)} , \tag{49}$$

but the enthalpy difference of the coolant flow, $\Delta \dot{H}_{DI}^{HM}$, comprises also an enthalpy flow of evaporation, as one part of the coolant is evaporated to humidify the air stream. The coolant temperature at the humidifier outlet is calculated as a function of the lumped temperature as

$$T_{DI}^{HM\,Out} = 2 \cdot T_{DI}^{HM} - T_{DI}^{PS\,Out} . \tag{50}$$

The convective heat flow term, $\dot{Q}_{Conv}^{B2DI(HM)}$, is modeled analogously to Eqn. 47 as

$$\dot{Q}_{Conv}^{B2DI(HM)} = (hA)_{B2DI(HM)} \cdot (T_B - T_{DI}^{HM}) , \tag{51}$$

where the heat transfer coefficient of the humidification section is assumed to be equal to the heat transfer coefficient of the power section,

$$h_{B2DI(HM)} = h_{B2DI(PS)} = h_{B2DI} . \tag{52}$$

Parameter Identification

Apart from the coefficients of the voltage equation, five parameters have to be determined experimentally. The nozzle constant of the cathode, k_p, can be determined by substituting data of the cathode inlet pressure, the cathode outlet pressure, and the air mass flow rate into Eqn. 40. The resulting value and its average are shown in Fig. 9 against experiment time. The parameter k_p was set to take the average experimental value.

In order to identify the pressure difference between anode and cathode, Δp_{AnCa}, data of the anode pressure and the cathode pressure have to be available. Since these pressures are not measured, they were defined as the mean values of the inlet and outlet pressures. In favor of a measurement data reduction, the pressure difference could also be approximated by the difference of the anode and cathode inlet pressures, or it could even be taken directly from the gas supply control settings. The experimental pressure difference and its average value are shown in Fig. 10 against experiment time. The parameter Δp_{AnCa} was set to take the average experimental value.

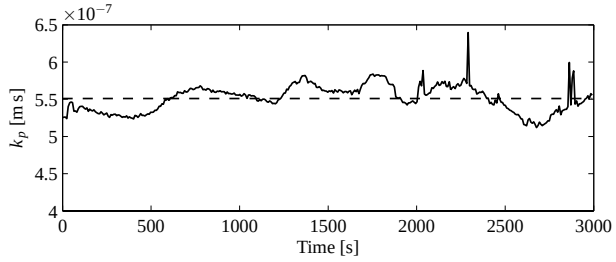

Figure 9. CATHODE NOZZLE CONSTANT: EXPERIMENT (–) AND AVERAGE VALUE (- -).

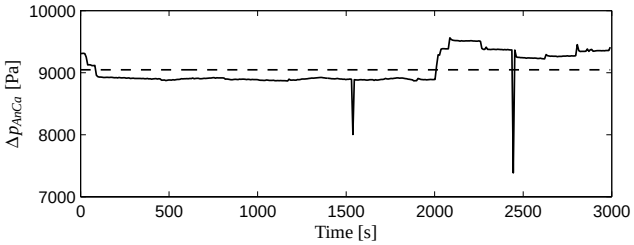

Figure 10. PRESSURE DIFFERENCE ANODE-CATHODE: EXPERIMENT (–) AND AVERAGE VALUE (- -).

In order to determine the heat transfer coefficient from the block to the coolant, h_{B2DI}, for different mass flow rates, the experimental data was split into tree sections. For the three sections, each with approximately constant coolant mass flow rate (compare Fig. 3), the heat transfer coefficient was varied to match the simulated with the measured coolant outlet temperature. The resulting values are shown in Fig. 11, represented by small squares. For this parameter identification, at least the following data is required: the stack current, the coolant mass flow rate, the coolant inlet and outlet temperatures, the cathode inlet and outlet temperatures. The accuracy of the resulting value can be improved by using also experimental data for the stack voltage, the air mass flow rate, and the cathode inlet pressure and relative humidity. Note, as indicated in the sensitivity analysis section, only slight inaccuracy in the coolant temperature or coolant mass flow measurement can lead to large deviation in the identified heat transfer parameter. In a subsequent step, the parameters K_h and δ_h were determined by curve fitting (Fig. 11).

The cathode temperature parameter k_T was determined by

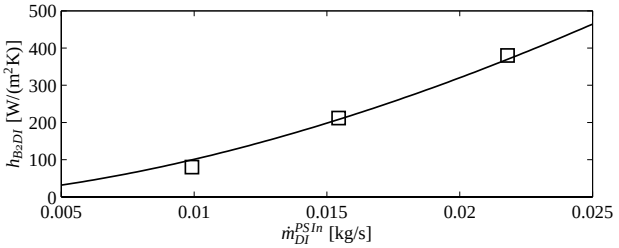

Figure 11. HEAT TRANSFER COEFFICIENT: IDENTIFICATION DATA (□) AND MODEL (–).

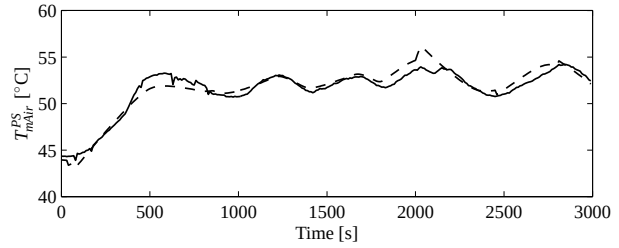

Figure 12. CATHODE TEMPERATURE: EXPERIMENT (–) AND MODEL (- -).

matching the predicted cathode temperature with the experimental cathode temperature. The result is shown in Fig 12. The experimental cathode temperature was defined as the average of the measured air temperature at the power section inlet and the measured air temperature at the power section outlet.

In Tab. 3, all parameters of the fuel cell system model are listed, except for the coefficients of the voltage equation. At the bottom of the table the values of the five experimentally determined parameters are specified. Most of the other parameters are geometrical parameters and thus determined in a straight forward fashion. The specific heat of the fuel cell system body, C_B, was calculated as the mass-weighted sum of the specific heats of the system components. The convective heat transfer coefficient, h_{B2Amb}, and the emissivity, ε, were estimated as already mentioned in the energy balance section.

Validation Results

The model parameters were identified based on the experimental data presented in Fig. 3. In order to show that the model can map the system behavior it has to be validated with a different set of experimental data. Therefore, the coolant outlet temperature was compared with the corresponding measurement data of two additional experimental runs. During these experiments the model input signals (electric current, coolant mass flow rate, and coolant inlet temperature) were varied for excitation of the system dynamics. The four constant input parameters of the model were chosen as follows:

Table 3. PARAMETERS OF THE FUEL CELL SYSTEM MODEL (EXCLUSIVE OF THE COEFFICIENTS OF THE VOLTAGE EQUATION).

Parameter	Value	Remark
n_{Cells}	24	
m_B	18 kg	
C_B	1300 J/(kg K)	Calculated
A_{B2Amb}	0.44 m^2	
h_{B2Amb}	3.9 W/(m^{2}K)	Estimated
ε	0.9	Estimated
A_{Active}	$296{\cdot}10^{-4}$ m^2	
λ_{Air}	2	
$m_{DI(PS)}$	0.51 kg	
$m_{DI(HM)}$	0.31 kg	
$A_{B2DI(PS)}$	0.75 m^2	
$A_{B2DI(HM)}$	0.5 m^2	
k_p	$5.5{\cdot}10^{-7}$ m s	Identified
k_T	340 W/K	Identified
Δp_{AnCa}	9200 Pa	Identified
K_h	$2.16{\cdot}10^5$ W/(m^{2}K)·(kg/s)$^{-1.67}$	Identified
δ_h	1.67	Identified

$$T_{Amb} = 25\,^{\circ}\mathrm{C}$$
$$T_{mAir}^{HMIn} = 20\,^{\circ}\mathrm{C}$$
$$T_{mH_2}^{PSIn} = 40\,^{\circ}\mathrm{C}$$
$$\dot{m}_{H_2O}^{mAirHMIn} = 0\,\mathrm{g/s}\ .$$

In Fig. 13 the results of the model validation are shown. During the first experiment the maximum prediction error is 1.4 K, whereas for the second experiment the maximum error is 2.3 K.

DISCUSSION AND CONCLUSIONS

A first-law control volume analysis and a sensitivity analysis have been performed for the PEM fuel cell system with integrated humidification section. The first-law energy balance and the H_2O mass balance for the gas channels were used to distinguish between relevant and negligible contributions to the thermal dynamics. It is shown that the enthalpy flow of the leaking hydrogen, the enthalpy flow of the purged moist hydrogen, and the mass flow of vapor on the anode side are of subordinate importance and thus negligible. The sensitivity analysis revealed the importance of sensor calibration on the control volume analysis of PEM fuel cell systems. Based on the preliminary investigations a control-oriented dynamic model of the fuel cell system was developed. The model predicts the bulk fuel cell transient temperature and voltage as a function of only three input sig-

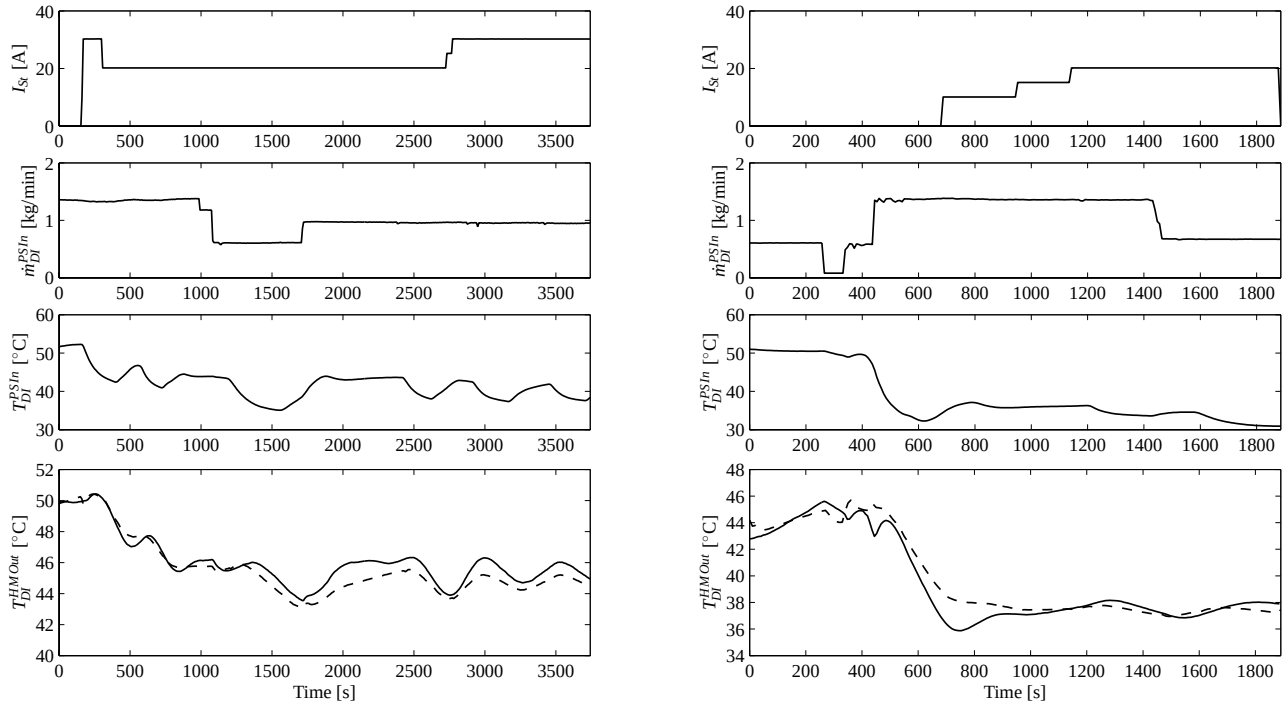

Figure 13. MODEL VALIDATION: IN EACH PLOT, SUBPLOTS 1–3 SHOW THE INPUT SIGNALS, SUBPLOT 4 THE COMPARISON BETWEEN EXPERIMENT (–) AND PREDICTION (- -) OF THE COOLANT OUTLET TEMPERATURE.

nals i.e., the current drawn, the coolant inlet temperature, and the coolant mass flow rate. Unlike other existing thermal models, it includes the gas supply system. The gas conditions thus do not appear as system inputs and therefore do not have to be provided through cumbersome measurements or another simulation model. The model is intended to be used for thermal control synthesis, performance simulations, or to be part of a coolant-loop simulation model. Despite its simplicity, the model predictions match the experimental data well, as shown in the validation section. The model was also designed to be applicable to different PEM fuel cell systems, as it comprises only a few parameters which are to be determined experimentally. With some adaptations, the model should also be usable for systems without an internal humidification section.

REFERENCES

[1] Amphlett, J. C., Mann, R. F., Peppley, B. A., Roberge, P. R., and Rodrigues, A., 1996. "A model predicting transient responses of proton exchange membrane fuel cells". Journal of Power Sources, **61** (1-2) , pp. 183–188.

[2] Lee, J. H., and Lalk, T. R., 1998. "Modeling fuel cell stack systems". Journal of Power Sources, **73** (2) , pp. 229–241.

[3] Xue, X., Tang, J., Smirnova, A., England, R., and Sammes, N., 2004. "System level lumped-parameter dynamic modeling of pem fuel cell". Journal of Power Sources, **133** (2) , pp. 188–204.

[4] Zhang, Y. J., Ouyang, M. G., Lu, Q. C., Luo, J. X., and Li, X. H., 2004. "A model predicting performance of proton exchange membrane fuel cell stack thermal systems". Applied Thermal Engineering, **24** (4) , pp. 501–513.

[5] Hrsg.: Verein Deutscher Ingenieure, 2002. *VDI-Wärmeatlas: Berechnungsblätter für den Wärmeübergang*. Springer, Berlin.

[6] Guzzella, L., 1999. Control oriented modelling of fuel-cell based vehicles. Presentation in NSF Workshop on the Integration of Modeling and Control for Automotive Systems.

[7] Amphlett, J. C., Baumert, R. M., Mann, R. F., Peppley, B. A., Roberge, P. R., and Rodrigues, A., 1994. "Parametric modeling of the performance of a 5-kw proton- exchange membrane fuel-cell stack". Journal of Power Sources, **49** (1-3) , pp. 349–356.

[8] Kim, J., Lee, S. M., Srinivasan, S., and Chamberlin, C. E., 1995. "Modeling of proton-exchange membrane fuel-cell performance with an empirical-equation". Journal of the Electrochemical Society, **142** (8) , pp. 2670–2674.

[9] Pukrushpan, J. T., Stefanopoulou, A. G., and Peng, H., 2004. *Control of Fuel Cell Power Systems: Principles, Modeling, Analysis and Feedback Design*. Springer, London.

Appendix: Voltage Equation

The single fuel cell operating voltage is defined as

$$V_{Cell} = E - v_{Act} - v_{Ohm} - v_{Conc}\,, \tag{53}$$

with the open circuit voltage,

$$\begin{aligned} E = {} & 1.229 - 8.5\cdot 10^{-4}(T_B - 298.15) \\ & + 4.308\cdot 10^{-5} T_B \left[\ln \frac{p_{H_2}^{PS}}{101325} + \frac{1}{2} \ln \frac{p_{O_2}^{PS}}{101325} \right]. \end{aligned} \tag{54}$$

The activation overvoltage is written as

$$v_{Act} = v_0 + v_a (1 - e^{-c_1 i})\,, \tag{55}$$

with coefficients defined as follows:

$$\begin{aligned} v_0 = {} & 0.279 - 8.5\cdot 10^{-4}(T_B - 298.15) \\ & + 4.308\cdot 10^{-5} T_B \left[\ln \left(\frac{p_{mAir}^{PS} - p_{Sat}}{101325} \right) \right. \\ & \left. + \frac{1}{2} \ln \left(\frac{0.1173 (p_{mAir}^{PS} - p_{Sat})}{101325} \right) \right] \end{aligned} \tag{56}$$

$$\begin{aligned} v_a = {} & 10^{-5}(1.8\cdot 10^{-4} T_B - 0.166) \left(\frac{p_{O_2}^{PS}}{0.1173} + p_{Sat} \right) \\ & + 10^{-10}(-1.618\cdot 10^{-5} T_B + 1.618\cdot 10^{-2}) \\ & \cdot \left(\frac{p_{O_2}^{PS}}{0.1173} + p_{Sat} \right)^2 \\ & + (-5.8\cdot 10^{-4} T_B + 0.5736) \end{aligned} \tag{57}$$

$$c_1 = 10\,. \tag{58}$$

The ohmic overvoltage is calculated as

$$v_{Ohm} = i R_{Ohm}\,, \tag{59}$$

with

$$R_{Ohm} = \frac{t_m}{\sigma_m} \tag{60}$$

$$t_m = 0.0125 \tag{61}$$

$$\sigma_m = b_1 \exp\left(b_2 \left(\frac{1}{303} - \frac{1}{T_B} \right) \right) \tag{62}$$

$$b_1 = 0.005139\,\lambda_m - 0.00326 \tag{63}$$

$$b_2 = 350\,. \tag{64}$$

The concentration overvoltage is written as

$$v_{Conc} = i \left(c_2 \frac{i}{i_{Max}} \right)^{c_3}\,, \tag{65}$$

with the following coefficients:

$$c_2 = \begin{cases} 10^{-5}(7.16\cdot 10^{-4} T_B - 0.622) \left(\dfrac{p_{O_2}^{PS}}{0.1173} + p_{Sat} \right) \\ \quad + (-1.45\cdot 10^{-3} T_B + 1.68)\,, \\ \quad \text{for } \left(\dfrac{p_{O_2}^{PS}}{0.1173} + p_{Sat} \right) < 2.0265\cdot 10^5 \\ 10^{-5}(8.66\cdot 10^{-5} T_B - 0.068) \left(\dfrac{p_{O_2}^{PS}}{0.1173} + p_{Sat} \right) \\ \quad + (-1.6\cdot 10^{-4} T_B + 0.54)\,, \\ \quad \text{for } \left(\dfrac{p_{O_2}^{PS}}{0.1173} + p_{Sat} \right) \geq 2.0265\cdot 10^5 \end{cases} \tag{66}$$

$$i_{Max} = 2.2 \tag{67}$$

$$c_3 = 2\,. \tag{68}$$

T_B is the temperature of the fuel cells, p_{mAir}^{PS} is the cathode pressure, p_{Sat} is water saturation pressure, which is a function of the respective temperature, and $p_{H_2}^{PS}$ and $p_{O_2}^{PS}$ are the partial pressures of oxygen in the cathode and of hydrogen in the anode, respectively.